NANO LETTERS

Letter

pubs.acs.org/NanoLett

# Quantifying van der Waals Interactions in Layered Transition Metal Dichalcogenides from Pressure-Enhanced Valence Band Splitting

Penghong Ci,[†,‡,§] Yabin Chen,[†,‡] Jun Kang,[‡] Ryuji Suzuki,[∥] Hwan Sung Choe,[†] Joonki Suh,[†] Changhyun Ko,[†] Taegyun Park,[†] Ke Shen,[†,§] Yoshihiro Iwasa,[∥] Sefaattin Tongay,[⊥] Joel W. Ager, III,[‡] Lin-Wang Wang,[‡] and Junqiao Wu*[,†,‡,§]

[†]Department of Materials Science and Engineering, University of California, Berkeley, California 94720, United States

[‡]Materials Sciences Division, Lawrence Berkeley National Laboratory, Berkeley, California 94720, United States

[§]Tsinghua-Berkeley Shenzhen Institute, University of California, Berkeley, California 94720, United States

[∥]Quantum-Phase Electronics Centre (QPEC) and Department of Applied Physics, University of Tokyo, Tokyo 113-8656, Japan

[⊥]School for Engineering of Matter, Transport, and Energy, Arizona State University, Tempe, Arizona 85287, United States

Supporting Information

**ABSTRACT:** van der Waals (vdW) forces, despite being relatively weak, hold the layers together in transition metal dichalcogenides (TMDs) and play a key role in their band structure evolution, hence profoundly affecting their physical properties. In this work, we experimentally probe the vdW interactions in $MoS_2$ and other TMDs by measuring the valence band maximum (VBM) splitting ($\Delta$) at $K$ point as a function of pressure in a diamond anvil cell. As high pressure increases interlayer wave function coupling, the VBM splitting is enhanced in 2H-stacked $MoS_2$ multilayers but, due to its specific geometry, not in 3R-stacked multilayers, hence allowing the interlayer contribution to be separated out of the total VBM splitting, as well as predicting a negative pressure (2.4 GPa) where the interlayer contribution vanishes. This negative pressure represents the threshold vdW interaction beyond which neighboring layers are electronically decoupled. This approach is compared to first-principles calculations and found to be widely applicable to other group-VI TMDs.

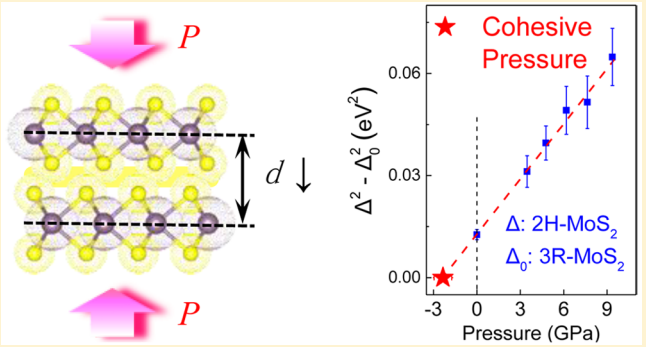


**KEYWORDS:** *van der Waals interaction, 3R-stacked $MoS_2$, spin−orbital coupling, interlayer wave function coupling, diamond anvil cell*

In layered materials, such as graphite and transition metal dichalcogenides (TMDs), van der Waals (vdW) force holds together the neighboring atomic layers. Despite being relatively weak, the vdW forces play a key role in the physical behavior of these materials, including forming van Hove singularities,[1] enabling unconventional quantum Hall effect,[1] evolving band structures, and facilitating anomalous lattice vibrations.[2,3] Therefore, gauging and controlling the vdW interactions are essential for understanding the physics of layered materials.

Atomic force microscope (AFM) is a traditional method to directly measure the vdW interactions between the AFM tip at the end of the cantilever and the sample surface via the oscillation frequency shift of the cantilever.[4−6] It has been successfully applied to study the vdW interactions between Pt−Pt metal contacts and between rare gas atoms.[4,7] For layered materials such as TMDs and graphene, even though AFM can measure their in-plane Young's modulus and other mechanical parameters,[8] it shows very limited capability in measuring the force and potential between the neighboring atomic layers. In light of this limitation, another technique has been reported in which pressure-sensitive molecules are encapsulated between neighboring layers, and the Raman shift of these molecules is used to determine the pressure experienced by the molecules sandwiched between the neighboring layers.[9−13] Pressures of ∼1.2 GPa were thus reported to be present in multilayer graphene based on the Raman shift of trapped molecules with sizes of ∼1 nm.[9] However, it is known that the equilibrium distance between graphene layers is only ∼0.3 nm, and the vdW interactions drop rapidly with increase in the interlayer separation;[14] therefore, it is not clear whether the pressure sensed by these ∼1 nm-sized molecules accurately reflects the native vdW pressure between the neighboring layers.

Here, we demonstrate a completely new method of gauging the vdW pressure in group-VI TMDs by tuning the valence band maximum (VBM) splitting at the $K$ point using a

**Received:** May 23, 2017
**Revised:** June 26, 2017
**Published:** June 28, 2017





DOI: 10.1021/acs.nanolett.7b02159
*Nano Lett.* 2017, 17, 4982−4988

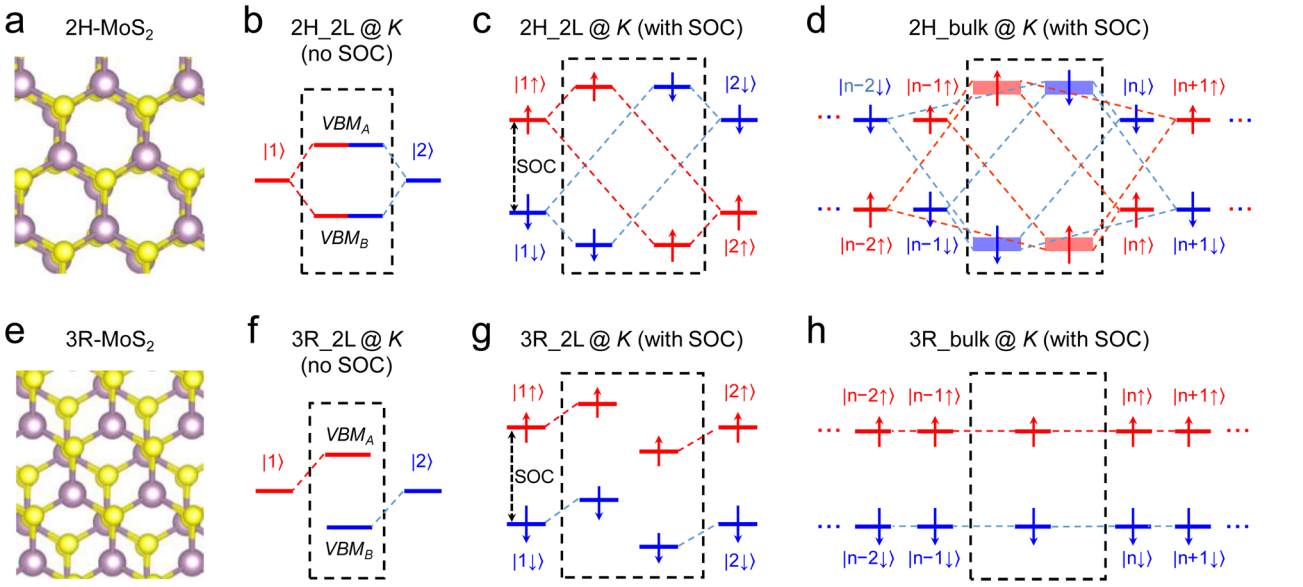


**Figure 1.** Mechanisms of VBM splitting at *K* point. (a,e), Schematic of layer stacking (top view). (b–d), (f–h), VBM splitting at the *K* point in the Brillouin zone for 2H- and 3R-$MoS_2$ with SOC and without SOC. Optical transitions from the two split VBM states to the CBM are responsible for the A and B exciton resonances observed in optical spectra. The purple and yellow spheres in a and e represent Mo and S atoms, respectively. The 2L stands for two layer. Arrows mean spin polarization. The $|1\rangle$ and $|2\rangle$ are wave functions states of VBM in two neighboring single layers.

diamond anvil cell (DAC). The VBM splitting is derived from interlayer wave function coupling and hence is sensitive to external pressure in 2H-$MoS_2$ but not in 3R-$MoS_2$ owing to the specific stacking geometry in the latter. We developed an analytical model to explain the difference in VBM splitting between 2H- and 3R-$MoS_2$ as a function of pressure. On the basis of the orbital bonding physics and the Morse potential, the model well explains the experimental results and quantifies the cohesive pressure in 2H-$MoS_2$. The results are found to be consistent with the value from first-principles calculations, and this approach is also generalized to other TMDs.

Both the 2H and 3R $MoS_2$ consist of identical S–Mo–S single layers, but with different stacking order. The 2H-stacked $MoS_2$ has a hexagonal symmetry with two S–Mo–S monolayer per unit cell, and the Mo (S) atoms in each layer reside upon the S (Mo) atoms of its neighboring layers,[15,16] as shown in Figure 1a and Figure S1a. In contrast, in the 3R-stacked $MoS_2$ having a rhombohedral symmetry and units consisting of three S–Mo–S monolayers, the Mo atoms of the middle layer sit above the S atoms of the bottom layer but below the hollow sites of the top one, as shown in Figure 1e and Figure S1b,c. It is clear that the inversion symmetry is broken in 3R-stacked $MoS_2$ but not in 2H-stacked ones.[15−17] The different atomic configuration and symmetry in these two structures have profound consequence on their physical properties especially related to valleytronics.[17]

We start with analyzing the topmost valence bands at the vertices (*K* and *K*′ points) of the hexagonal Brillouin zone in the simplified case, that is, without considering spin–orbital coupling (SOC). In this case, for monolayer $MoS_2$, the VBM at the *K* point is degenerate.[17,18] But when two monolayers are stacked together to form a bilayer structure held together by weak vdW interactions, the VBM at *K* point splits into two states, $VBM_A$ and $VBM_B$ (Figure 1b,f), in both cases of 2H stack and 3R stack but with totally different mechanisms. The interlayer interactions include interlayer wave function coupling (analogous to covalent bonding) and interlayer dipole effects (analogous to ionic bonding). The former can be understood as a bonding/antibonding process that arises from the fact that electron clouds from neighboring layers overlap, thereby leading to the VBM splitting.[1,17] The latter originates from environmental difference for atoms in neighboring layers, leading to formation of an interlayer electric dipole and subsequently electrostatic potential difference between neighboring layers.[17] Figure S1a,b shows wave functions of the states at the *K* point in the cases of 2H and 3R stacking. In the 2H stacking, the $VBM_A$ and $VBM_B$ states both come from mixed wave functions of both the upper ($|1\rangle$) and lower ($|2\rangle$) layers, indicating the mechanism of interlayer wave function coupling behind the VBM splitting. We have also obtained the wave functions $|1\rangle$ and $|2\rangle$ from DFT calculations and found nonzero wave function overlap $\langle 1|2\rangle$, confirming the existence of interlayer VBM coupling in the 2H structure. The identical atomic environment for Mo atoms residing in different layers leads to identical local potential for these layers, and hence there is no interlayer dipole formation in 2H-stacked bilayer or bulk. In stark contrast, in 3R-stacked bilayers the Mo atom in the top layer has a distinct atomic environment from the one in the bottom layer, leading to formation of interlayer dipoles and an electrostatic potential energy difference between the two layers. This is the origin of VBM splitting in bilayer 3R-$MoS_2$. In 3R-stacked $MoS_2$, the $VBM_A$ state at *K* point is exclusively from the bottom layer $|1\rangle$ and $VBM_B$ state is exclusively from the top layer $|2\rangle$, as shown in Figure S1b, indicating that the wave functions of the two VBM states are localized in the individual layers. The DFT calculated wave function overlap $\langle 1|2\rangle = 0$, and therefore, the interlayer wave function coupling makes no contribution to the split of VBM at the *K* point in 3R structure. In short, without considering the SOC the VBM splitting in bilayer 2H-$MoS_2$ results from interlayer wave function coupling, while interlayer dipole formation is the reason for the VBM splitting in bilayer 3R-$MoS_2$.

When the SOC arising from d orbitals of the metal ions is considered, the VBM splitting at the *K* point is shown in Figure 1c,g. For monolayer $MoS_2$, because of the broken inversion symmetry, the VBM at the *K* valley splits into two sub-bands,[19]



DOI: 10.1021/acs.nanolett.7b02159
Nano Lett. 2017, 17, 4982–4988

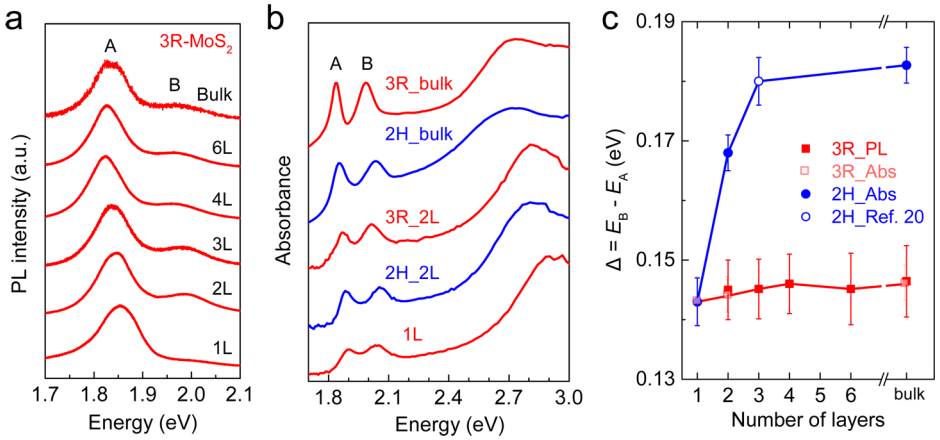


**Figure 2.** Measured layer dependent exciton resonance energies ($E_B$ and $E_A$). (a) Normalized PL spectra of 3R-$MoS_2$ of different number of layers. (b) Absorbance spectra of 2H- and 3R-$MoS_2$. (c) $E_B - E_A$ in both 2H- and 3R-$MoS_2$ as a function of number of layers.

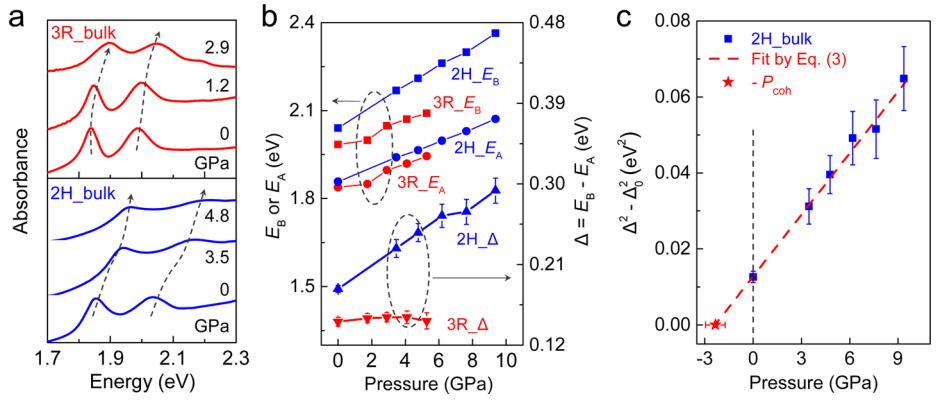


**Figure 3.** Evolution of $\Delta = E_B - E_A$ with pressure. (a) Absorbance spectra of bulk 2H- and 3R-$MoS_2$ under pressure (dashed lines and arrows indicate transitions associated with $E_A$ and $E_B$). (b) $E_B$, $E_A$, and $\Delta$ of the bulk as a function of pressure. (c) Fit of $\Delta^2 - \Delta_0^2$ versus pressure for bulk 2H-$MoS_2$ by eq 3. $\Delta_0$ is $E_B - E_A$ of 3R-$MoS_2$.

which host opposite spin polarizations. The spin polarization at the $K'$ valley is the opposite to that at the $K$ valley.[18,19] In 2H-stacked $MoS_2$ bilayers (Figure 1c), its upper VBM ($VBM_A$) at the $K$ point is mixed with both spin-up and spin-down states of both the top and bottom single layers ($|1\uparrow\rangle$ and $|2\downarrow\rangle$), because inversion symmetry is restored in the 2H bilayers, removing spin polarization of the upper and lower bands in the VBM.[17−19] Therefore, in 2H bilayers the total amount of VBM splitting is attributed to a combination of intralayer SOC and interlayer wave function coupling. Increasing the layer number or application of external pressure enhances the interlayer coupling of wave functions, efficiently increasing the VBM splitting. This effect was experimentally observed and summarized in Figures 2c and 3b. Figure 2b,c presents the absorbance spectra of monolayer, bilayer, and bulk 2H-$MoS_2$ in which the VBM splitting, the energy difference between the excitons B and A ($\Delta = E_B - E_A$), rises with the increase in the number of layers. This result is also consistent with previous reports.[20−22] As the interlayer wave function coupling occurs primarily between nearest neighboring layers only, bulk 2H-$MoS_2$ is expected to show similar VBM splitting scheme and pressure dependence as that of 2H-$MoS_2$ bilayers, shown in Figures 1d, 3b, and S4d.

The 3R-stacked $MoS_2$, however, shows completely different physics of VBM splitting. The VBM splitting in 3R-$MoS_2$ bilayers (Figure 1g) is attributed to intralayer SOC and the interlayer dipole effects. However, we note that the interlayer dipole effects do not affect the value of $\Delta = E_B - E_A$ measured in 3R bilayers, because optical transitions occur mainly within the same layer in which the $VBM_A$ and $VBM_B$ energies just shift altogether by the interlayer dipole effects without being widened apart (Figure 1g). More interestingly, going from the 3R bilayer to 3R bulk, even the interlayer dipoles disappear. This is because unlike 3R bilayers, in 3R bulk all the Mo atoms now become equivalent (Figure S1c) in terms of their atomic environment, so that the interlayer dipoles and the resultant splitting disappear. This analysis is also supported by angle-resolved photoelectron spectroscopy study of the valence bands of bulk 3R-$MoS_2$.[17] Owing to the lack of inversion symmetry (as in the monolayer case), 3R-stacked $MoS_2$ even in the bulk hosts spin-polarized upper and lower valence bands. Because of the absence of interlayer wave function coupling, the measured $\Delta = E_B - E_A$ in 3R-$MoS_2$ is insensitive to both applied pressure and the number of layers in stark contrast to 2H-$MoS_2$. Therefore, $\Delta$ in 3R-$MoS_2$ could be utilized as baseline to extract the interlayer contribution from the total $\Delta$ in 2H-$MoS_2$. The analysis of the difference between 3R (crystal structure was determined by Laue picture in Figure S2) and 2H crystals is verified by experimental data shown in Figures 2c and 3b.

It is known that the states of VBM and CBM are mostly composed of ($d_{x^2-y^2}$, $d_{xy}$) and $d_{z^2}$ orbitals of the Mo atoms,



DOI: 10.1021/acs.nanolett.7b02159
Nano Lett. 2017, 17, 4982−4988

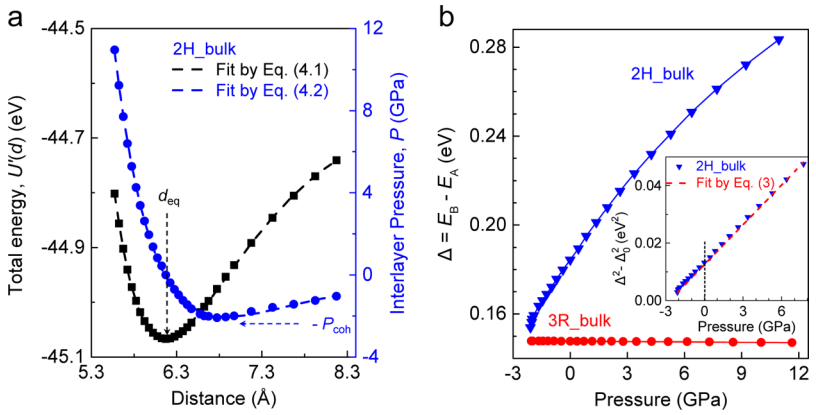


**Figure 4.** DFT calculation of interlayer interaction and VBM splitting. (a) DFT calculated total energy per unit cell and vdW pressure in bulk 2H-$MoS_2$ as a function of interlayer distance. Lines are fits to eqs 4.1 and 4.2. (b) Evolution of $\Delta = E_B - E_A$ with pressure from DFT calculations. Lines are guide to the eye. Inset: Fit to the calculated $\Delta^2 - \Delta_0^2$ as a function of pressure using eq 3.

respectively.[18] Because the Mo atoms lie in the middle of the sandwich structure of single layer, they are screened by the S atoms and have less influence on the interlayer coupling. This can explain that the energy of exciton A ($E_A$) in 3R-$MoS_2$ is almost independent of the number of layers, shown in the photoluminescence (PL) spectra in Figure 2a. 2H-$MoS_2$ also shows a similar trend for $E_A$, which has been reported in literature.[22] Despite the insensitivity of $E_A$ with thickness, both 2H-$MoS_2$ in literature and 3R-$MoS_2$ in our experiments show that $E_A$ has a small but recognizable blueshift from multilayer to monolayers, which can be understood from a simple quantum confinement effect.

Now we turn to the pressure behavior of these materials. Pressure is expected to enhance the VBM splitting of 2H-$MoS_2$ by increasing the interlayer overlap of the wave functions but not so much in 3R-$MoS_2$ and monolayer $MoS_2$. Indeed, as shown in Figures 3a,b, S4, and S5c, the VBM splitting ($\Delta = E_B - E_A$) is found to be strongly dependent on pressure in bilayer and bulk 2H-$MoS_2$, consistent with a previous report on the VBM splitting of few-layer 2H-$MoS_2$ versus layer spacing,[23,24] but nearly independent of pressure in monolayers and 3R-$MoS_2$ (bilayer or bulk). Such difference in $\Delta$ between 2H- and 3R-$MoS_2$ allows us to separate the contribution of interlayer coupling out of the total VBM splitting. Here, monolayer $MoS_2$ was also measured in Figure S4 to probe the pressure effect of VBM splitting attributed purely to intralayer interactions, which shows very small pressure dependence, akin to the behavior of 3R-$MoS_2$ bulk. This is expected from the model discussed in Figure 1. However, the data of bulk 3R-$MoS_2$ (as opposed to monolayers) was utilized in this work as the baseline ($\Delta_0$) for decoupling the interlayer and intralayer contributions to $\Delta$. This is because the bulk sample ensures that the pressure medium solely mechanically transmits the pressure without significant effects of chemical reaction or charge transfer with the sample, which may potentially occur in the case of monolayers. Figure 3 also shows that in 2H and 3R samples, $E_A$ rises with the increase of pressure, which is consistent with DFT calculations shown in Figure S5a. This trend is explained by the enhanced repulsion between the d orbitals of Mo atoms and p orbitals of S atoms, in response to the contraction of the Mo−S bonds under the hydrostatic pressure.[25]

Next, we decouple the interlayer and intralayer contributions to $\Delta$. When two separated single layers of $MoS_2$ are approaching each other in the 2H stacking, their electron wave functions start to overlap across the vdW gap, resulting in an equilibrium distance ($d_{eq}$) that separates the regimes of attraction ($d > d_{eq}$) and repulsion ($d < d_{eq}$), as shown in Figure 4a. We model the energetics of this process using the formation of bonding/antibonding states in dissimilar diatomic molecules. The "atomic" orbital energies are $E_{A0}$ and $E_{B0}$, respectively, corresponding to the upper and lower edges of the VBM at the $K$ point ($VBM_A$ and $VBM_B$) in monolayer $MoS_2$. The eigenvalues are given by solving the following secular equation

$$\begin{vmatrix} E - E_{A0} & V \\ V & E - E_{B0} \end{vmatrix} = 0 \tag{1}$$

where $V$ is the interaction introduced between $E_{A0}$ and $E_{B0}$ by the wave function overlap. The difference between the two eigen energies, $\Delta = E_B - E_A$, is given by

$$\Delta^2 - \Delta_0^2 = 4V^2 \tag{2}$$

where $\Delta_0 = E_{B0} - E_{A0}$ is the VBM split in monolayer $MoS_2$ caused by SOC alone, which has the same value and pressure-independence as those of bulk 3R $MoS_2$. It can be shown (see below) that $V^2$ varies linearly with externally applied pressure, that is

$$\Delta^2 - \Delta_0^2 = G(P + P_{coh}) \tag{3}$$

where the pressure $P_{coh}$, hereon termed as the cohesive pressure, represents the threshold vdW pressure that needs to be overcome in mechanical exfoliation of the 2H-$MoS_2$ layers from bulk crystals (Figure 4a). It is also the negative pressure at which the interlayer distance is sufficiently large that the neighboring layers are nearly electronically decoupled, such that $\Delta \approx \Delta_0$. Figure 3c plots the experimentally measured $\Delta^2 - \Delta_0^2$ as a function of $P$, which indeed shows a linear relationship, extrapolating to $P_{coh} = 2.4 \pm 0.6$ GPa for bulk 2H-$MoS_2$.

In order to analyze and probe the physics behind the relationship between $\Delta$ and $P$, we discuss this based on the Morse potential that is typically used to model interatomic forces in molecules. The Morse potential energy is written as[26]

$$U(d) = U_{depth}\left[1 - \exp\left(-\frac{d - d_{eq}}{d_{width}}\right)\right]^2 \tag{4.1}$$



DOI: 10.1021/acs.nanolett.7b02159
Nano Lett. 2017, 17, 4982−4988

where $U_{depth}$ is the depth of the potential, $d_{width}$ is the width of the potential well, and $d_{eq}$ is the equilibrium distance. The interatomic force is given by

$$F(d) = -\frac{\partial U}{\partial d} = -2\frac{U_{depth}}{d_{width}}\left[1 - \exp\left(-\frac{d - d_{eq}}{d_{width}}\right)\right]\exp\left(-\frac{d - d_{eq}}{d_{width}}\right) \quad (4.2)$$

Here the potential energy between two neighboring layers $U(d)$ is half of that per unit cell $U'(d)$ (shown in the Figure 4a), that is, $U_{depth} = U'_{depth}/2$. $F(d)$ is zero when $d = d_{eq}$. Moreover, $F(d)$ takes an extreme at $d = d_{eq} + d_{width}$ ln2, where $F = F_{coh} = U'_{depth}/4d_{width}$, corresponding to the maximum cohesive force that needs to be overcome to dissociate the molecule. Fitting this potential to the first-principles calculated interlayer interactions (per unit cell) in 2H-$MoS_2$, we find excellent agreement as shown in Figure 4a. In Figure 4a, the force is converted to interlayer pressure via $P(d) = F(d)/S$, where $S$ is the basal area of the unit cell in the 2H-$MoS_2$, hence $P_{coh} = U'_{depth}/4Sd_{width}$. The best-fit values for $U_{depth}$, $d_{width}$, and $d_{eq}$ are 0.44 eV, 1.02 Å, and 6.16 Å, respectively.

Next, we assume that the interaction matrix element $V$ in a bilayer is proportional to the overlap integral of the wave functions from the two layers (mostly p orbitals of the sulfur atoms from the two layers), that is, $V \propto \langle 1|2\rangle$,[27] where $|1\rangle$ and $|2\rangle$ denote the electronic states of the VBM at $K$ point from the upper and lower layer, respectively. Because the atomic radial wave functions have an exponential decay behavior,[28] it is reasonable to assume that the overlap integral of the wave functions also follows the functional form of the Morse potential and rapidly decays at the same length scale of $d_{width}$

$$V = V_0 e^{-d/d_{width}} \quad (5)$$

Combining eqs 4.2 and 5, one obtains

$$\Delta^2 - {\Delta_0}^2 = V_0^2 \exp\left(-2\frac{d_{eq}}{d_{width}}\right)\left[\frac{1}{2}\left(1 + \sqrt{\frac{P + P_{coh}}{P_{coh}}}\right)\right]^2 \quad (6)$$

In the limit of $P \gg P_{coh}$, it follows that

$$\Delta^2 - {\Delta_0}^2 \approx \frac{V_0^2}{4P_{coh}} \exp\left(-2\frac{d_{eq}}{d_{width}}\right)(P + P_{coh})$$

which reduces to the linear pressure dependence as shown by eq 3. Specifically, the linear pressure dependence of $\Delta^2 - {\Delta_0}^2$ extrapolates to zero at $P = -P_{coh}$, where $\Delta \approx \Delta_0$, that is, the VBM splitting $\Delta = E_B - E_A$ of the 2H-$MoS_2$ returns to the value of monolayers or bulk 3R-$MoS_2$. Such linear extrapolation was performed on both the experimental and first-principles calculated data, as shown in Figures 3c and 4b, respectively. $P_{coh}$ thus obtained from the experimental data is 2.4 ± 0.6 GPa, which is in consistency with the first-principles calculated value (2.0 GPa) in Figure 4b, and is also close to the value directly determined from the extreme of the calculated pressure in Figure 4a. These consistencies justify our assumptions and approach of determining $P_{coh}$ from the VBM splitting. We note that although the linear $\Delta^2 \sim P$ relation hold mathematically only when $P \gg P_{coh}$, both experimental (Figure 3c) and calculated data (Figure 4b) show that the linearity holds for smaller $P$ values.

This approach is obviously universally applicable to other group-VI 2H-stacked TMD materials that have similar origin of VBM splitting at the $K$ point. Compared to other stacking orientations, the 2H stacking order is predominantly the most widely used one in research and design of devices due to its smallest layer distance, lowest energy, and most stable structure.[1] Absorbance spectra of bulk 2H-$WS_2$ and 2H-$MoSe_2$ were also measured under pressure, as shown in Figures S6 and S7 in the Supporting Information. Comparing to their VBM splitting in monolayers ($\Delta_0$) reported in the literature,[21] we obtain their pressure dependence of $\Delta^2 - {\Delta_0}^2$. Similar linear extrapolation leads to $P_{coh}$ values of 2.5 ± 0.7 GPa in 2H-$WS_2$ and 3.0 ± 1.2 GPa in 2H-$MoSe_2$, both of which are consistent with DFT calculated results (1.95 and 2.07 GPa, respectively) as shown in Figures S6 and S7. We note that within the error bar the cohesive pressure of the three TMD materials are close, especially for $MoS_2$ (2.4 ± 0.6 GPa) and $WS_2$ (2.5 ± 0.7 GPa). This is attributed to the fact that the interactions between neighboring layers are mostly dictated by the wave functions overlap integral of the chalcogen atoms and are relatively insensitive to the metal atoms. Therefore, the overlap integral of the S atom in these two materials should be very similar, resulting in similar cohesive force values. Compared to $MoS_2$ and $WS_2$, $MoSe_2$ has chalcogen atoms (Se) with larger atomic radius, which enhances the overlap of their electron clouds, giving rise to slightly higher cohesive pressure (3.0 ± 1.2 GPa). This approach is also potentially able to parametrize the interlayer force−distance curve in TMDs. Figure 4a shows that the Morse potential model describes the potential energy by three parameters, that is, $U_{depth}$, $d_{width}$, and $d_{eq}$. Here $d_{eq}$ can be obtained by thickness measurements, and the other two parameters can be determined from the cohesive force ($F_{coh} = U_{depth}/2d_{width}$) measured in this paper and the out-of-plane Young's modulus ($Y_\perp = -2U_{depth}/(d_{width})^2$) reported by Gao et al.[29] Therefore, in principle, combining the measured $Y_\perp$, $d_{eq}$, and $F_{coh}$, it is possible to experimentally determine the interlayer force−distance and potential energy−distance curves in TMDs.

In conclusion, the VBM splitting in TMDs manifests the intralayer spin−orbital coupling as well as interlayer wave function overlap. High-pressure experiments were performed to tune the wave function coupling in multilayer TMDs with different stackings and compared to that of the monolayers. Their different pressure dependence allows separation of the interlayer contribution from the intralayer spin−orbital coupling. The negative pressure obtained from extrapolating the pressure dependence gives the maximum cohesive pressure of the TMDs, which is the threshold pressure one needs to overcome to mechanically exfoliate the multilayers, as well as the separation pressure to electronically decouple neighboring layers. The results were supported with DFT calculations and a universally applicable analytical model. This study thus provides a general approach that can be used to experimentally gauge and determine the interlayer vdW interactions in TMDs for theoretical guidance and practical applications.

**Methods.** *DFT Calculations.* The calculations were performed using the Vienna ab initio simulation package (VASP).[30] The generalized gradient approximation of Perdew−Burke−Ernzerhof (GGA-PBE)[31] was adopted for the exchange-correlation functionals. The energy cutoff for the plane-wave expansion was set to 400 eV. Structure relaxation was stopped when the force on each atom was smaller than 0.005 eV/Å. The vdW interaction was included by using the D3 correction scheme of Grimme.[32]



DOI: 10.1021/acs.nanolett.7b02159
Nano Lett. 2017, 17, 4982−4988

*Sample Preparation.* The bulk samples were exfoliated from bulk crystals, and monolayer and bilayer samples were prepared by the gold-mediated exfoliation method.[33]

*Optical and Thickness Measurements.* Raman and PL spectra were measured by a Raman/PL spectrometer (Renishaw Inc.) with a 488 nm laser as the excitation source. In the absorbance measurements, the radiation light from a Quartz Tungsten Halogen lamp source passed through Acton monochromator, chopper and pinhole, then was focused on the samples by a 20X long working distance objective lens; the photomultiplier tubes detector (R2368) was used to collect the transmitted light data. Sample thickness was characterized by an AFM (Veeco Inc.) in the tapping mode.

*Transfer of TMD Materials.* In order to explore the band structure evolution under high pressure in the DAC, the samples were transferred to the surface of diamond by the standard wet transfer techniques.[9,34] Briefly, PDMS covered an exfoliated $MoS_2$ on the $SiO_2$/Si substrate. Subsequently, the PDMS/$MoS_2$ was released from the substrate by etching the $SiO_2$ in a 2 mol/L KOH solution for about 2 h. After rinsing in deionized water to remove the KOH residue, the $MoS_2$ was transferred to the diamond surface.

*High-Pressure Measurements in the Diamond Anvil Cell.* The DAC is composed of a pair of diamond anvils with culet diameter of 200 $\mu$m and a gasket of thickness of about 30 $\mu$m, made of 304 stainless steel. Its optical image is shown in Figure S4a. The pressure transmission medium filled inside the pressure chamber is a mixture of methanol and ethanol with the volume ratio of 4:1. The standard ruby luminescence method was used to calibrate the pressure.[35]

## ■ ASSOCIATED CONTENT

### Supporting Information

The Supporting Information is available free of charge on the ACS Publications website at DOI: 10.1021/acs.nanolett.7b02159.

Wave functions of states and schematic of stacking of 2H- and 3R-$MoS_2$, optical characterization and Laue picture of a 3R-$MoS_2$ single crystal, Raman and absorbance spectra of 2H- and 3R-$MoS_2$ under pressure, measured and calculated $E_B$, $E_A$, and $E_B - E_A$ of bilayers as a function of pressure, total energy and vdW pressure in bulk 2H- $WS_2$ and $MoSe_2$ as a function of interlayer distance, and deviation of $\Delta^2 - \Delta_0^2 = 4\ V^2$ (PDF)

## ■ AUTHOR INFORMATION


### Corresponding Author

*E-mail: wuj@berkeley.edu.

### ORCID

Jun Kang: 0000-0003-4788-0028
Taegyun Park: 0000-0002-1138-8747
Joel W. Ager III: 0000-0001-9334-9751
Junqiao Wu: 0000-0002-1498-0148


### Author Contributions

P.C., Y.C., and J.K. contributed equally to this work.

### Notes

The authors declare no competing financial interest.

## ■ ACKNOWLEDGMENTS

This work was supported by the Electronic Materials Program at the Lawrence Berkeley National Laboratory, which is supported by the Office of Science, Office of Basic Energy Sciences, of the U.S. Department of Energy under Contract No. DE-AC02-05CH11231. J.W., P.C., and K.S. acknowledge support from Tsinghua-Berkeley Shenzhen Institute (TBSI). We are grateful for Chenhao Jin and Ming Chen of UC Berkeley and Zhiquan Yuan of Tsinghua University for helpful discussions.

## ■ ABBREVIATIONS

vdW: van der Waals
TMDs: transition metal dichalcogenides
VBM: valence band maximum
CBM: conduction band minimum
AFM: atomic force microscopy
DAC: diamond anvil cell
PL: photoluminescence

## ■ REFERENCES


(1) Liu, K.; Zhang, L.; Cao, T.; Jin, C.; Qiu, D.; Zhou, Q.; Zettl, A.; Yang, P.; Louie, S. G.; Wang, F. *Nat. Commun.* **2014**, *5*, 4966.
(2) Splendiani, A.; Sun, L.; Zhang, Y.; Li, T.; Kim, J.; Chim, C.-Y.; Galli, G.; Wang, F. *Nano Lett.* **2010**, *10* (4), 1271−1275.
(3) Lee, C.; Yan, H.; Brus, L. E.; Heinz, T. F.; Hone, J.; Ryu, S. *ACS Nano* **2010**, *4* (5), 2695−2700.
(4) Kawai, S.; Foster, A. S.; Björkman, T.; Nowakowska, S.; Björk, J.; Canova, F. F.; Gade, L. H.; Jung, T. A.; Meyer, E. *Nat. Commun.* **2016**, *7*, 11559.
(5) Lantz, M.; Hug, H.; Hoffmann, R.; Van Schendel, P.; Kappenberger, P.; Martin, S.; Baratoff, A.; Güntherodt, H.-J. *Science* **2001**, *291* (5513), 2580−2583.
(6) Sader, J. E.; Jarvis, S. P. *Appl. Phys. Lett.* **2004**, *84* (10), 1801−1803.
(7) Ternes, M.; González, C.; Lutz, C. P.; Hapala, P.; Giessibl, F. J.; Jelínek, P.; Heinrich, A. J. *Phys. Rev. Lett.* **2011**, *106* (1), 016802.
(8) Liu, K.; Yan, Q.; Chen, M.; Fan, W.; Sun, Y.; Suh, J.; Fu, D.; Lee, S.; Zhou, J.; Tongay, S. *Nano Lett.* **2014**, *14* (9), 5097−5103.
(9) Vasu, K. S.; Prestat, E.; Abraham, J.; Dix, J.; Kashtiban, R. J.; Beheshtian, J.; Sloan, J.; Carbone, P.; Neek-Amal, M.; Haigh, S. J.; et al. *Nat. Commun.* **2016**, *7*, 12168.
(10) Khestanova, E.; Guinea, F.; Fumagalli, L.; Geim, A.; Grigorieva, I. *Nat. Commun.* **2016**, *7*, 12587.
(11) Algara-Siller, G.; Lehtinen, O.; Wang, F.; Nair, R.; Kaiser, U.; Wu, H.; Geim, A.; Grigorieva, I. *Nature* **2015**, *519* (7544), 443−445.
(12) Aradhya, S. V.; Frei, M.; Hybertsen, M. S.; Venkataraman, L. *Nat. Mater.* **2012**, *11* (10), 872−876.
(13) Zamborlini, G.; Imam, M.; Patera, L. L.; Mentes, T. O.; Stojić, N. a.; Africh, C.; Sala, A.; Binggeli, N.; Comelli, G.; Locatelli, A. *Nano Lett.* **2015**, *15* (9), 6162−6169.
(14) Chen, X.; Tian, F.; Persson, C.; Duan, W.; Chen, N.-X. *Sci. Rep.* **2013**, *3*, 3046.
(15) Ye, M.; Winslow, D.; Zhang, D.; Pandey, R.; Yap, Y. K. In *Recent advancement on the optical properties of two-dimensional molybdenum disulfide (MoS2) thin films*; Photonics; Multidisciplinary Digital Publishing Institute, 2015; pp 288−307.
(16) Yan, J.; Xia, J.; Wang, X.; Liu, L.; Kuo, J.-L.; Tay, B. K.; Chen, S.; Zhou, W.; Liu, Z.; Shen, Z. X. *Nano Lett.* **2015**, *15* (12), 8155−8161.
(17) Suzuki, R.; Sakano, M.; Zhang, Y. J.; Akashi, R.; Morikawa, D.; Harasawa, A.; Yaji, K.; Kuroda, K.; Miyamoto, K.; Okuda, T.; et al. *Nat. Nanotechnol.* **2014**, *9* (8), 611−617.
(18) Fan, X.; Singh, D. J.; Zheng, W. *J. Phys. Chem. Lett.* **2016**, *7*, 2175−2181.
(19) Mak, K. F.; He, K.; Shan, J.; Heinz, T. F. *Nat. Nanotechnol.* **2012**, *7* (8), 494−498.
(20) Dhakal, K. P.; Duong, D. L.; Lee, J.; Nam, H.; Kim, M.; Kan, M.; Lee, Y. H.; Kim, J. *Nanoscale* **2014**, *6* (21), 13028−13035.




DOI: 10.1021/acs.nanolett.7b02159
*Nano Lett.* 2017, 17, 4982−4988

(21) Li, Y.; Chernikov, A.; Zhang, X.; Rigosi, A.; Hill, H. M.; van der Zande, A. M.; Chenet, D. A.; Shih, E.-M.; Hone, J.; Heinz, T. F. *Phys. Rev. B: Condens. Matter Mater. Phys.* **2014**, *90* (20), 205422.
(22) Mak, K. F.; Lee, C.; Hone, J.; Shan, J.; Heinz, T. F. *Phys. Rev. Lett.* **2010**, *105* (13), 136805.
(23) Zhang, Y.; Li, H.; Wang, H.; Liu, R.; Zhang, S.-L.; Qiu, Z.-J. *ACS Nano* **2015**, *9* (8), 8514−8519.
(24) Dou, X.; Ding, K.; Jiang, D.; Fan, X.; Sun, B. *ACS Nano* **2016**, *10* (1), 1619−1624.
(25) Kang, J.; Tongay, S.; Zhou, J.; Li, J.; Wu, J. *Appl. Phys. Lett.* **2013**, *102* (1), 012111.
(26) Konowalow, D. D. *Morse Potential Molecular Interactions*; University of Wisconsin-Madison, 1961.
(27) Hoffmann, R. *J. Chem. Phys.* **1963**, *39* (6), 1397−1412.
(28) Trambly de Laissardiere, G.; Mayou, D.; Magaud, L. *Nano Lett.* **2010**, *10* (3), 804−808.
(29) Gao, Y.; Kim, S.; Zhou, S.; Chiu, H.-C.; Nélias, D.; Berger, C.; De Heer, W.; Polloni, L.; Sordan, R.; Bongiorno, A. *Nat. Mater.* **2015**, *14* (7), 714−720.
(30) Kresse, G.; Furthmüller, J. *Phys. Rev. B: Condens. Matter Mater. Phys.* **1996**, *54* (16), 11169.
(31) Perdew, J. P.; Burke, K.; Ernzerhof, M. *Phys. Rev. Lett.* **1996**, *77* (18), 3865.
(32) Grimme, S.; Antony, J.; Ehrlich, S.; Krieg, H. *J. Chem. Phys.* **2010**, *132* (15), 154104.
(33) Desai, S. B.; Madhvapathy, S. R.; Amani, M.; Kiriya, D.; Hettick, M.; Tosun, M.; Zhou, Y.; Dubey, M.; Ager, J. W.; Chrzan, D. *Adv. Mater.* **2016**, *28* (21), 4053−4058.
(34) Geim, A. K.; Grigorieva, I. V. *Nature* **2013**, *499* (7459), 419−425.
(35) Mao, H.; Xu, J.-A.; Bell, P. *J. Geophys. Res.* **1986**, *91* (B5), 4673−4676.



DOI: 10.1021/acs.nanolett.7b02159
*Nano Lett.* 2017, 17, 4982−4988

**Supporting Information**

# Quantifying van der Waals Interactions in Layered Transition Metal Dichalcogenides from Pressure-Enhanced Valence Band Splitting

Penghong Ci,[1, 2,3] Yabin Chen,[1, 2] Jun Kang,[2] Ryuji Suzuki,[4] Hwan Sung Choe,[1] Joonki Suh,[1] Changhyun Ko,[1] Taegyun Park,[1] Ke Shen,[1,3] Yoshihiro Iwasa,[4] Sefaattin Tongay,[5] Joel W. Ager III,[2] Lin-Wang Wang[2] and Junqiao Wu[1,2,3*]

[1]Department of Materials Science and Engineering, University of California, Berkeley, California 94720, United States
[2] Materials Sciences Division, Lawrence Berkeley National Laboratory, Berkeley, California 94720, United States
[3]Tsinghua-Berkeley Shenzhen Institute, University of California, Berkeley, California 94720, United States
[4]Quantum-Phase Electronics Centre (QPEC) and Department of Applied Physics, University of Tokyo, Tokyo 113-8656, Japan
[5]School for Engineering of Matter, Transport and Energy, Arizona State University, Tempe, Arizona 85287, United States
[*]E-mail: wuj@berkeley.edu

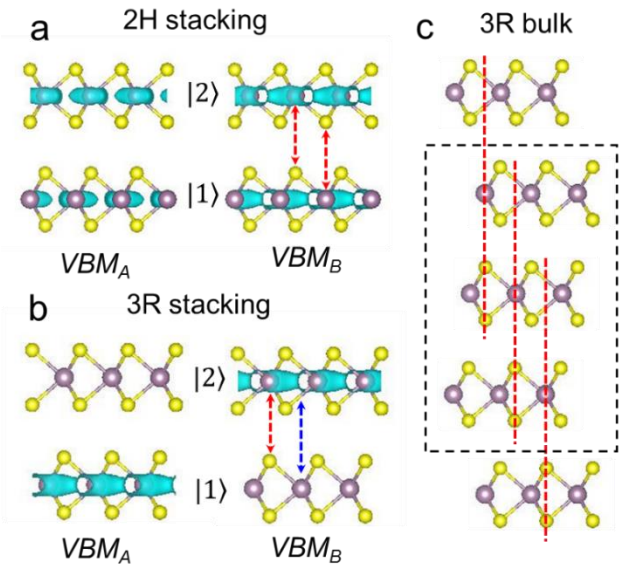


**Figure S1.** (a) and (b) wavefunctions of states at the K point in 2H and 3R stacking. (c) schematic of stacking (side view) of bulk 3R-$MoS_2$.

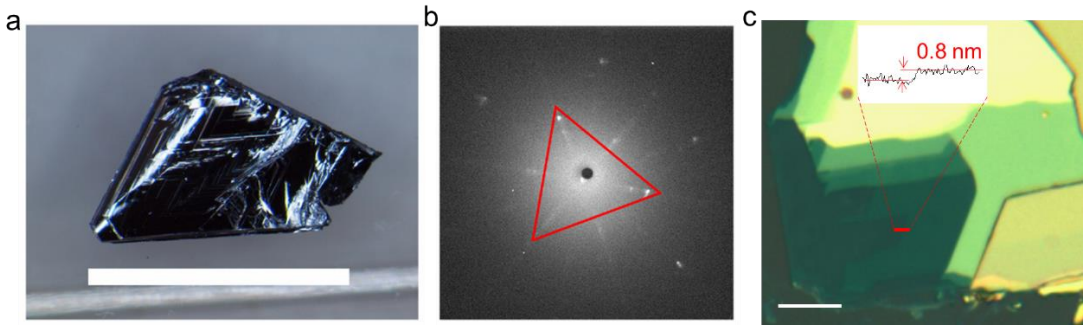


**Figure S2.** (a) Optical characterization of a 3R-$MoS_2$ single crystal. Scale bar, 2 mm. (b) Laue picture of this 3R-$MoS_2$ single crystal. (c) Representative optical micrograph of the exfoliated crystal. Inset: AFM height image. Scale bar, 20 μm.

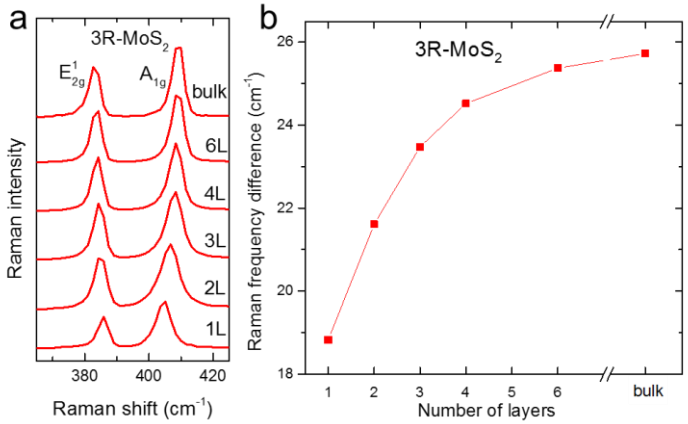


**Figure S3.** Layer dependent Raman spectra of 3R-$MoS_2$. (a) Raman spectra of 3R-$MoS_2$ with different number of layers. (b) Wavenumber difference between the $A_{1g}$ and $E^1_{2g}$ modes in 3R-$MoS_2$ as a function of number of layers.

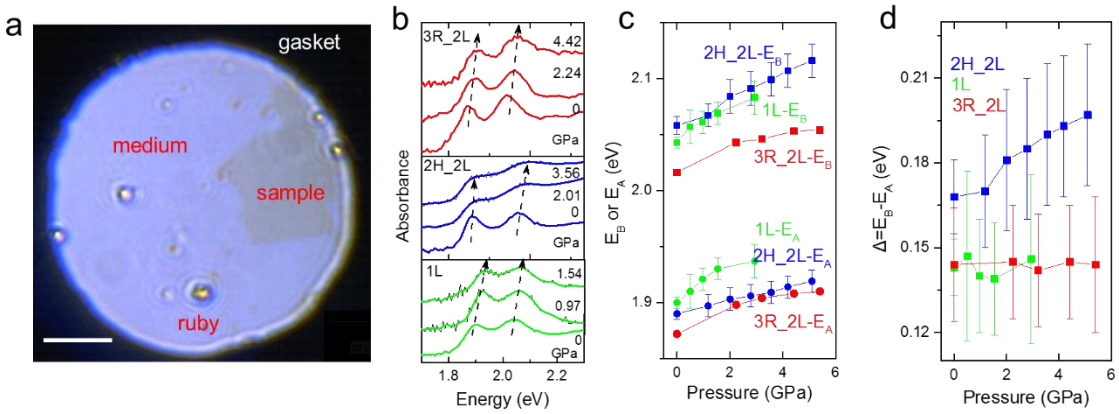


**Figure S4.** (a) Microscope image (top view) of the pressure chamber in the DAC. Scale bar, 20 um. (b) Absorbance spectra of bilayer 2H- and 3R-$MoS_2$ under pressure. (c) and (d) $E_B$, $E_A$ and $E_B$-$E_A$ of the bilayers as a function of pressure.

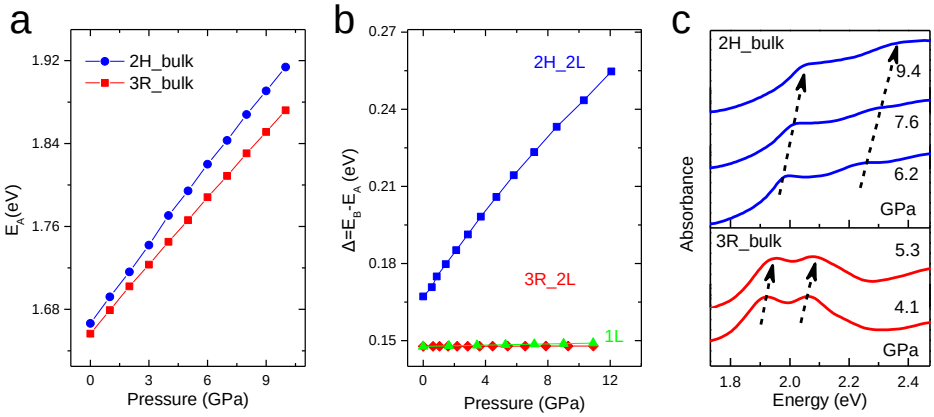


**Figure S5.** Evolution of $E_A$ (a) and $E_B$-$E_A$ (b) with pressure as calculated by DFT. (c) Absorbance spectra of bulk 2H- and 3R-$MoS_2$ under pressure by experiment.

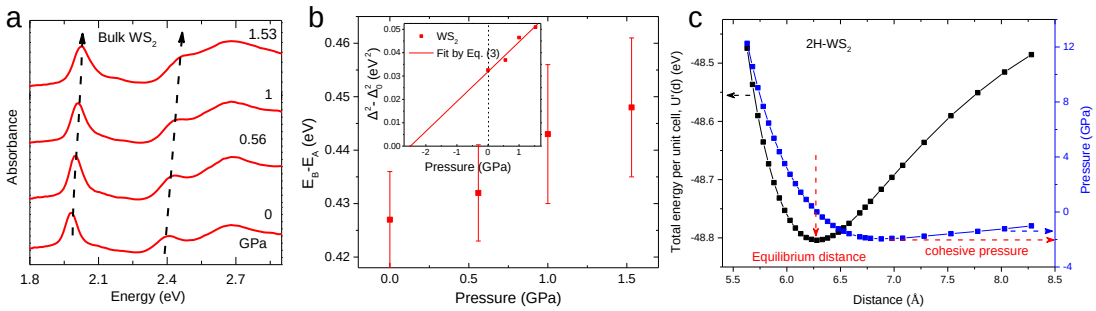


**Figure S6.** (a) Absorbance spectra of bulk 2H-$WS_2$ under pressure. (b) $E_B$-$E_A$ as a function of pressure. Inset: Fit of $\Delta^2$-$\Delta_0^2$ as a function of pressure for bulk 2H-$WS_2$. (c) Total energy and vdW pressure in bulk 2H-$WS_2$ as a function of interlayer distance.

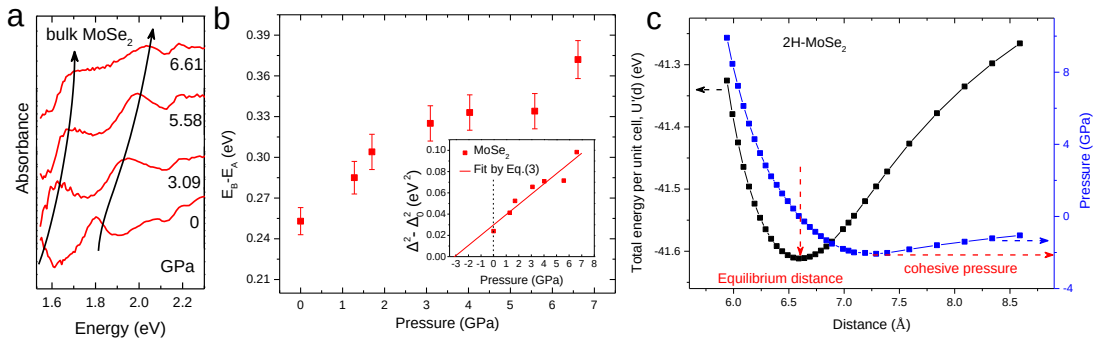


**Figure S7.** (a) Absorbance spectra of bulk 2H-$MoSe_2$ under pressure. (b) $E_B$-$E_A$ as a function of pressure. Inset: Fit of $\Delta^2$-$\Delta_0{}^2$ as a function of pressure for bulk 2H-$MoSe_2$. (c) Total energy and vdW pressure in bulk 2H-$MoSe_2$ as a function of interlayer distance.

**Note 1.** Deviation of $\Delta^2 - \Delta_0{}^2 = 4V^2$

In the main text of the manuscript, we modeled the energies of the pressure modulation using the formation of bonding/antibonding states in dissimilar diatomic molecules. The "atomic" orbital energies are $E_{A0}$ and $E_{B0}$, respectively, corresponding to the upper and lower edges of the VBM at the *K* point ($VBM_A$ and $VBM_B$) in monolayers (namely, in the situation without interlayer coupling). The eigenvalues are given by solving the following secular equation,

$$\begin{vmatrix} E - E_{A0} & V \\ V & E - E_{B0} \end{vmatrix} = 0$$

where *V* is the interaction introduced between $E_{A0}$ and $E_{B0}$ by the interlayer wavefunction overlap.

Solving the above equation, we can obtain the two eigenvalues for the interacted VBMs,

$VBM_A$ is $E_A = (E_{A0} + E_{B0}) + \frac{1}{2}\sqrt{(E_{A0} - E_{B0})^2 + 4V^2}$ and

VBMB is $E_B = (E_{A0} + E_{B0}) - \frac{1}{2}\sqrt{(E_{A0} - E_{B0})^2 + 4V^2}$.

Hence,

$E_A - E_B = \sqrt{(E_{A0} - E_{B0})^2 + 4V^2}$,

that is,

$(E_A - E_B)^2 - (E_{A0} - E_{B0})^2 = 4V^2$.

As stated in the manuscript, we define $|E_A - E_B|$ and $|E_{A0} - E_{B0}|$ as $\Delta$ and $\Delta_0$, respectively. In this way, we obtain $\Delta^2 - \Delta_0{}^2 = 4V^2$, which is Eq. (2) in the manuscript. Later in the manuscript, we connect *V* with pressure *P*, hence leading to an equation linking the experimentally measurable $\Delta$ (*P*) relation, which was used for the extrapolation to obtain the cohesive pressure.